

Logic-Embedded Vectors for Intracellular Partitioning, Endosomal Escape, and Exocytosis of Nanoparticles

Rita E. Serda,* Aaron Mack, Anne L. van de Ven, Silvia Ferrati, Kenneth Dunner, Jr., Biana Godin, Ciro Chiappini, Matthew Landry, Louis Brousseau, Xuewu Liu, Andrew J. Bean, and Mauro Ferrari

A new generation of nanocarriers, logic-embedded vectors (LEVs), is endowed with the ability to localize components at multiple intracellular sites, thus creating an opportunity for synergistic control of redundant or dual-hit pathways. LEV encoding elements include size, shape, charge, and surface chemistry. In this study, LEVs consist of porous silicon nanocarriers, programmed for cellular uptake and trafficking along the endosomal pathway, and surface-tailored iron oxide nanoparticles, programmed for endosomal sorting and partitioning of particles into unique cellular locations. In the presence of persistent endosomal localization of silicon nanocarriers, amine-functionalized nanoparticles are sorted into multiple vesicular bodies that form novel membrane-bound compartments compatible with cellular secretion, while chitosan-coated nanoparticles escape from endosomes and enter the cytosol. Encapsulation within the porous silicon matrix protects these nanoparticle surface-tailored properties, and enhances endosomal escape of chitosan-coated nanoparticles. Thus, LEVs provide a mechanism for shielded transport of nanoparticles to the lesion, cellular manipulation at multiple levels, and a means for targeting both within and between cells.

Prof. R. E. Serda, A. Mack, Dr. A. L. van de Ven, S. Ferrati, Dr. B. Godin, M. Landry, Prof. L. Brousseau, Prof. X. Liu, Prof. M. Ferrari
Department of NanoMedicine and Biomedical Engineering
University of Texas Health Science Center
1825 Pressler Street, Suite 537, Houston, TX 77030, USA
E-mail: rita.serda@uth.tmc.edu

K. Dunner, Jr.
High Resolution Electron Microscopy Facility
University of Texas M. D. Anderson Cancer Center
Houston, TX 77030, USA

C. Chiappini
Department of Biomedical Engineering
The University of Texas at Austin
Austin, TX 78712, USA

DOI: 10.1002/sml.201000727

Prof. A. J. Bean
Department of Neurobiology and Anatomy
University of Texas Health Science Center
Houston, TX 77030, USA

Prof. A. J. Bean
Department of Pediatrics
University of Texas M. D. Anderson Cancer Center
Houston, TX 77030, USA

Prof. M. Ferrari
Department of Experimental Therapeutics
University of Texas M. D. Anderson Cancer Center
Houston, TX 77030, USA

Prof. M. Ferrari
Department of Bioengineering
Rice University
Houston, TX 77005, USA

1. Introduction

Nanoparticles, with the capacity for cell-specific delivery of therapeutics and imaging agents, have the potential for organelle-specific targeting following cellular internalization. Examples include nuclear targeting with carbon nanospheres,^[1] quantum dots,^[2] and gold nanoparticles,^[3] as well as cytoplasmic localization of cationic polystyrene nanoparticles.^[4] For therapeutic applications, the majority of drug targets reside within cells; however, the ability to treat a given target is limited by target accessibility and pathway redundancy. Effective therapeutics therefore require innovative strategies to overcome these barriers. Newer-generation nanoparticles, which include logic-embedded vectors (LEVs), are higher-order particles with the potential for targeting multiple intracellular sites with synergistic therapeutics or theranostics containing both imaging and therapeutic modalities.

The majority of nanoparticles and microparticles are internalized into membrane-bound compartments known as endosomes and phagosomes. As these vesicles mature, their contents are sorted and packaged for discrete destinations,^[5,6] which include intracellular organelles such as the nucleus, the cytosol, and exocytosis^[7] or transcytosis from the cell. Secretion of vesicular contents can occur at different stages of the endo-lysosomal pathway. For example, the protein Niemann–Pick C1 (NPC1) is required for secretion of amine-rich contents from the lysosome,^[8] and may therefore function in secretion/exocytosis of amine-modified nanoparticles from lysosomes. A variety of cells, including dendritic cells, macrophages, reticulocytes, lymphocytes, and endothelial cells, secrete microvesicles, microparticles, and exosomes constitutively.^[9,10] The mechanisms for cellular release are unique, with microvesicles being generated by shedding of the plasma membrane,^[10,11] microparticles being formed by membrane blebbing during apoptosis,^[10,12] and exosomes originating from intracellular vesicles contained within multivesicular bodies (MVBs) derived from sorting endosomes.^[10,13,14] Exosomes, also referred to as antigen-presenting vesicles, are reported to be 40–90 nm in size, while microvesicles are 100–200 nm and microparticles are 80–1200 nm.^[10] It is reported that cellular secretion of exosomes allows for the transfer of microRNAs, messenger RNA (mRNA), and various proteins (e.g., major histocompatibility complex (MHC) class I and II) out of the cell, potentially enabling cell–cell communication.

Reports of endosomal escape of nanoparticles include systems containing: cationic polymers, such as polyethylenimine;^[15,16] pH-sensitive polymers, such as poly(propylacrylic acid)^[17,18] and *N*-isopropylacrylamide-*co*-propylacrylic acid;^[19] and enzyme-targeting peptides, such as collagen-mimetic peptides.^[20] Cytoplasmic delivery of nanoparticles, and their associated payloads, allows for silencing of specific genes at the level of mRNA translation. In this study we introduce LEVs with the ability to perform two distinct, primary functions in target cells owing to intracellular partitioning of particles into unique organelles. In one embodiment, LEVs target both the late endosome and cytoplasm, and in another reach perinuclear vesicles but also release subpopulations that are secreted from the cell (**Figure 1**). These latter results

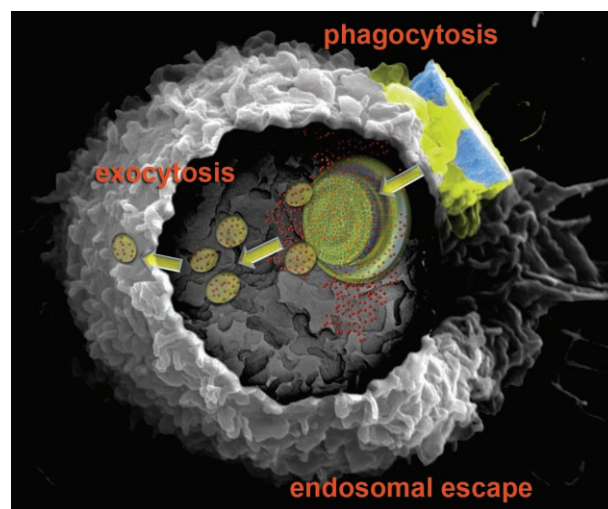


Figure 1. Artistic rendition of a scanning electron microscopy image of a macrophage showing particle phagocytosis, intracellular partitioning of particles, endosomal escape, and exocytosis of nanoparticle-loaded vesicles.

pave the way for the development of LEVs that deliver a signaling payload to be communicated by a target cell to its cellular neighbors.

2. Results

2.1. Cellular Internalization of Silicon Particles

For assembly of the LEV, we chose to use discoidal silicon particles, fabricated by our group using standard photolithography and electrochemical etching.^[21,22] Particles with a diameter of $3.2 \pm 0.2 \mu\text{m}$, pore size $51.3 \pm 28.7 \text{ nm}$, and 80% porosity (**Figure 2a**) were chosen based on preliminary studies which showed high loading efficiency with 10-nm superparamagnetic iron oxide nanoparticles (SPIONs).^[23] J774 murine macrophages were used to study cellular uptake and intracellular trafficking of particles. Scanning electron microscopy (SEM) images provide an example of early microparticle uptake with cellular lamellopodia emerging to encircle surface-adherent particles (**Figure 2b**). During the internalization step, the particle is shown oriented perpendicular to the cell membrane.

Live confocal imaging confirmed rapid (within 3 min of microparticle introduction) uptake of DyLight 594-modified silicon microparticles by macrophages using CellTracker Green for cell imaging (**Figure 2c**). Images were acquired every 3 min. The internalized particles migrated to the perinuclear region of the cell, as suggested by the co-localization of nuclear and particle-associated fluorophores beginning 12.5 min after the introduction of silicon particles. The corresponding movie is included in the Supporting Information. Ultrastructural examination of J774 cells, by transmission electron microscopy (TEM), 15 min after silicon particle introduction illustrates phagocytosis of particles and their subsequent localization in the perinuclear region of the cell (**Figure 2d**).

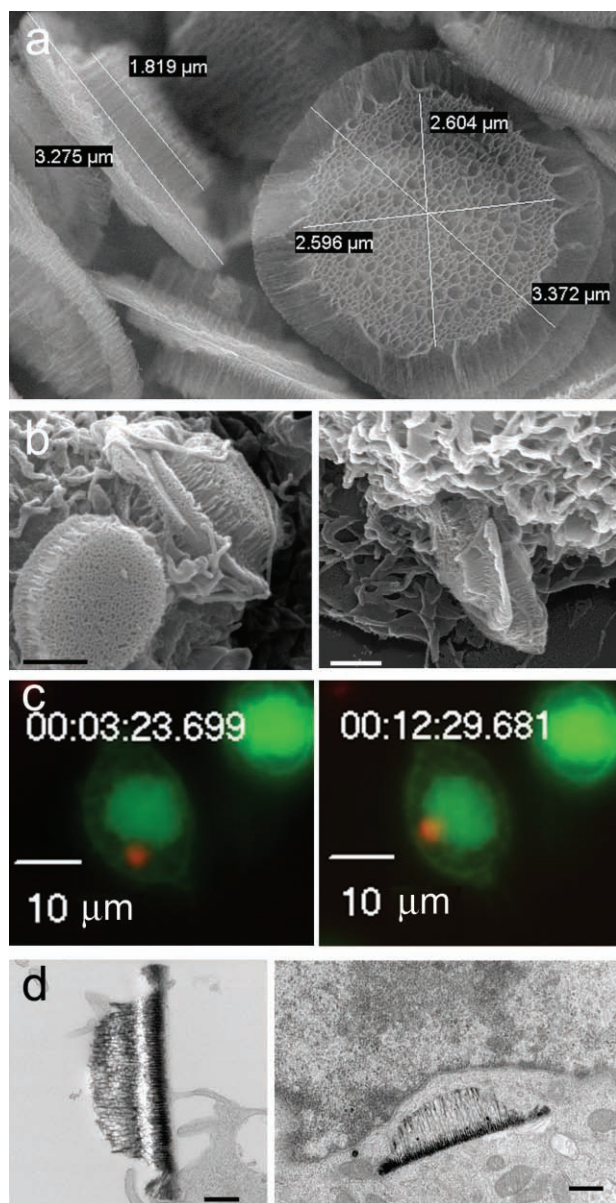


Figure 2. Phagocytosis and intracellular trafficking of silicon particles. a) SEM image of silicon microparticles. b) SEM images show particles being internalized by macrophages (scale bars: 1 μm ; left 30 k, right 50 k magnification). c,d) Both live confocal imaging (c) and TEM (d) show internalized particles migrating to the perinuclear region of macrophages (scale bars: 500 nm).

2.2. Particle Characterization and Loading Potential

To determine the impact of SPION surface modification on loading the nanoparticles into the porous matrix of oxidized silicon particles, silicon particles were loaded with carboxylated or amine- or chitosan-coated SPIONs (coated in the presence of 0.6 mg mL^{-1} chitosan) and examined by SEM at increasing magnifications (Figure 3a). Carboxylated SPIONs were not retained in the porous matrix following washing, while both amine- and chitosan-coated SPIONs were found in abundance. The arrow in the first column indicates a single carboxylated SPION located within the pores. The zeta

potential, which is the electrokinetic potential directly related to the net surface electrical charge of each particle formulation, is given in Figure 3b. Zeta potential measurements were performed in acidic buffer (pH 5.0) to increase the stability of the chitosan coating and to mimic loading conditions. Both the oxidized silicon particles and carboxylated SPIONs were negatively charged whereas amine-modified and chitosan-coated SPIONs had a positive charge (20.5 and 26.1, respectively). The change in SPION zeta potential, from -27.4 to 26.1 mV, that accompanied chitosan coating of carboxylated SPIONs supports surface coating with positively charged chitosan. Chitosan is a biodegradable polysaccharide composed of random β -(1–4)-linked D-glucosamine and N-acetyl-D-glucosamine units. It was chosen as a coating for SPIONs based on its biocompatibility, high charge density, and reports of its potential use for intracytoplasmic delivery of drugs and nanoparticles.^[24]

Fourier transform infrared (FTIR) spectra were acquired for each SPION formulation and for chitosan (Figure 3c). FTIR spectroscopy measures the frequency and intensity associated with each functional group and indicates the presence of specific groups and changes in molecular structure that occur upon complex formation. Amine-modified SPIONs, which contain oleic acid, polyethylene glycol (PEG), and amine groups, displayed characteristic N–H spectral bands near 3300 cm^{-1} , while the spectra of carboxy-SPIONs displayed prominent C=O and C–H bands near 1700 and 2900 cm^{-1} , respectively. The spectrum from 86% deacetylated chitin exhibited characteristic amide bands at 1605 and 1504 cm^{-1} . These characteristic bands shifted to 1646 and 1532 cm^{-1} following association of chitosan (0.6 mg mL^{-1}) with SPIONs. The shift in energies indicates that chitosan association with carboxylated SPIONs involves amide bond formation.

2.3. Optimization of Chitosan Coating

While carboxylated SPIONs had a negative zeta potential (-27 mV , borate buffer; -22 mV , acetic acid), the zeta values became increasingly positive after being coated in 0.01 – 0.24 mg mL^{-1} chitosan solutions (Figure 4a). This increase is attributed to positive chitosan polymers being adsorbed to the particle surface. The zeta potential remained positive, but dropped from 31.7 mV at 0.24 mg mL^{-1} chitosan to an average of 20 mV at chitosan concentrations of 0.60 mg mL^{-1} and higher in borate buffer. The drop in zeta potential may reflect more SPIONs on the surface of smaller nanoparticles.

Chitosan-coated particles tended to form large aggregates at concentrations of chitosan that coincided with the change in charge polarity of the negative SPIONs (i.e., at the point of nearest neutrality throughout the particle; Figure 4b). At this point of charge reversal, the molar ratio of SPIONs to chitosan was 1:89 (the mass ratio was 1:0.2). The average particle diameter, based on dynamic light scattering (DLS), was 521 nm , as compared to an average DLS size of 155 nm at concentrations of chitosan of 0.24 mg mL^{-1} and higher, thus confirming aggregation of the 30-nm

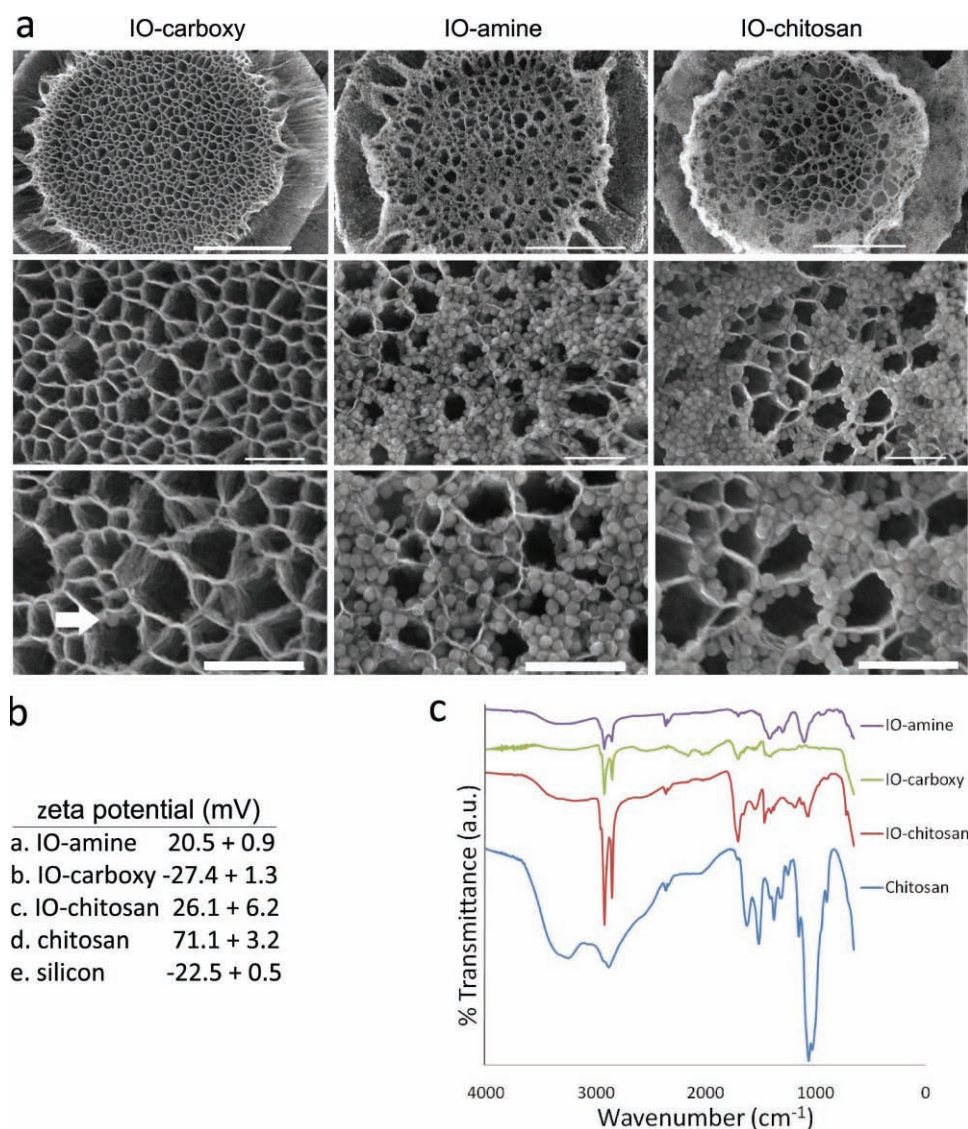


Figure 3. Characterization of particles. a) Oxidized silicon microparticles loaded with three surface variants (carboxylated, amine, chitosan) of 30-nm SPIONs (IO; magnification: 25 k, 120 k, 200 k; scale bars: top row 1 μm , others 200 nm). b) Zeta potential of each particle formulation in borate buffer, pH 5.0. c) FTIR spectra of SPIONs and chitosan.

chitosan-coated SPIONs. SEM measurements of particle diameter for individual particles coated with 0–0.13 mg mL^{-1} chitosan (Supporting Information, Figure 1) were not significantly different. However, the mean particle diameter increased from 26.4 ± 2.9 (uncoated) to 31.5 ± 2.8 nm when coated with 1.0 mg mL^{-1} chitosan ($n = 20$; $p < 0.000002$).

To quantitatively determine the amount of chitosan bound to SPIONs at each coating concentration, a colorimetric assay based on the affinity of chitosan for dyes was performed.

The protonated amino groups of chitosan attract anionic dyes, such as Congo Red. The absorbance spectra of amine- and chitosan-coated SPIONs in the presence of Congo Red (absorbance 520 nm) are shown in Figure 4c. The linear relationship between dye absorbance and concentration was used to calculate the amount of chitosan bound to a fixed number

of particles (Figure 4d). The amount of bound chitosan per particle increased when coated with chitosan concentrations from 0.01 to 1 mg mL^{-1} , and then reached a plateau at higher concentrations. At 1.0 mg mL^{-1} of chitosan and higher, 10 μg of chitosan was bound to 5 μg of SPIONs, which yielded a mass ratio of 1:2 SPIONs to chitosan. Zeta potential and DLS measurements were consistent with the finding that the amount of bound chitosan on purified SPIONs remains unchanged at concentrations of chitosan of 1 mg mL^{-1} and higher.

FTIR spectra acquired at each chitosan coating concentration support a change in the intensity of all major spectral bands at chitosan concentrations of 0.06 mg mL^{-1} and higher (Figure 4e). Spectral bands in SPIONs coated in solutions of 0–0.02 mg mL^{-1} chitosan remained small with 96–99% transmittance. The appearance of a broadband at 3200–3400 cm^{-1} in SPIONs coated with 0.06–3 mg mL^{-1} chitosan indicated

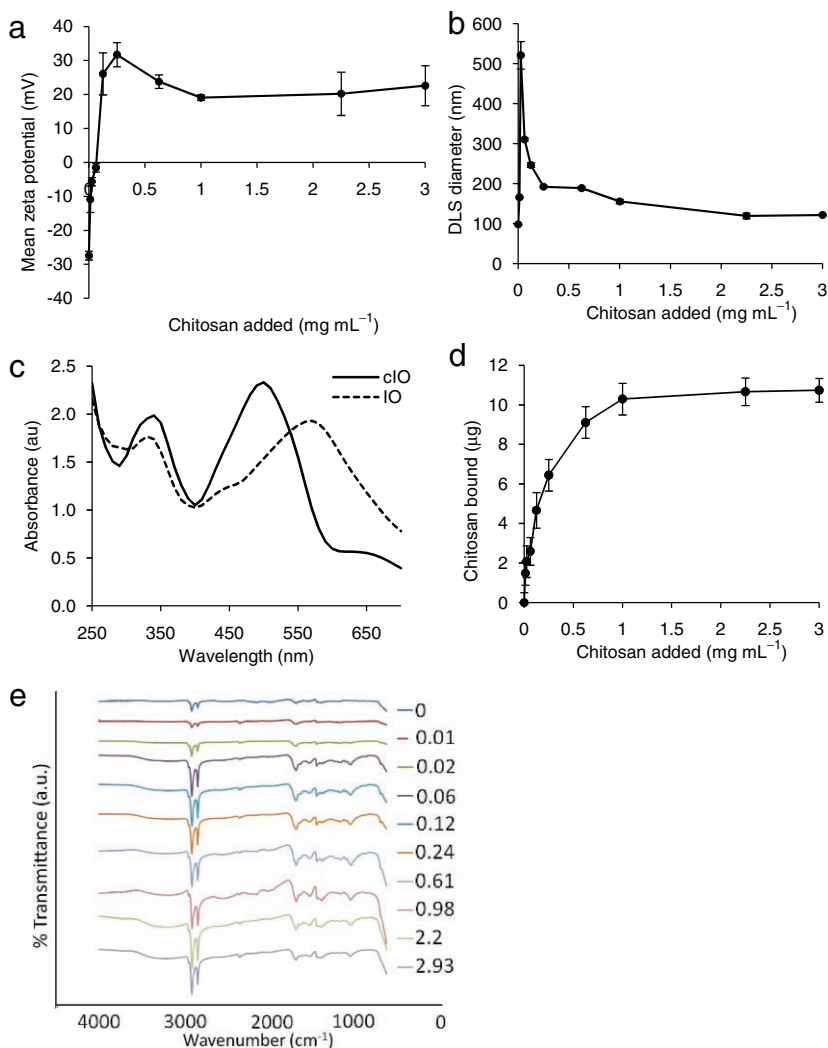


Figure 4. Characterization of chitosan coatings on SPIONs. a,b) Effect of chitosan concentration on zeta potential (a) and size (b) of SPIONs. c) Absorbance spectra of amine- (IO) and chitosan-coated (cIO) SPIONs in the presence of Congo Red (absorbance 520 nm). d) Colorimetric assay showing the effect of chitosan concentration on particle coating. e) FTIR transmission spectra of SPIONs coated with 0–3 mg mL⁻¹ of chitosan.

an increase in the presence of H-bonds. Characteristic amide bands at 1530 cm⁻¹ and C–O stretching vibrations at 1060 cm⁻¹ in SPIONs coated with 0.06 mg mL⁻¹ chitosan and higher support the introduction of glucosamine units on the SPION surface.

2.4. Endosomal Escape of Chitosan-Coated Nanoparticles

Size and surface chemistry are known to modulate cellular uptake, intracellular trafficking, and cytotoxicity of particles. In this study, in addition to the two surface functionalities, we compared the intracellular trafficking of LEVs in which the silicon particles were loaded with 10-, 15-, or 30-nm SPIONs.

SPIONs were coated with 0.6 mg mL⁻¹ chitosan at a mass ratio of 1:0.5 (SPION:chitosan). Following cellular uptake, both 10- and 30-nm chitosan-coated SPIONs

were seen crossing the endosomal membrane. In the top row of **Figure 5**, black arrows designate SPIONs free in the cytoplasm 24 h after introduction of LEVs to macrophages.

We next evaluated the trafficking of chitosan-coated SPIONs over time by mapping particle location at 2, 24, and 48 h (Figure 5, bottom four images). Two hours after the introduction of LEVs, internalized LEVs were present in large vacuoles. In contrast to earlier images that showed chitosan nanoparticles in the cytoplasm at 24 h, LEVs more heavily loaded with nanoparticles were slower to release their cargo. Although some nanoparticles were seen in the cytoplasm, the majority were present in endosomes as clusters. At 48 h, grouped SPIONs were spatially removed from carrier silicon particles. The cell shown in Figure 5 at 48 h has a membrane surrounding the distal portion of the silicon particle and near SPIONs that remain adjacent to the silicon particle. However, no membrane can be seen surrounding the spatially removed SPIONs or surrounding the silicon particle proximal to the released SPIONs. The release of chitosan-coated SPIONs may result from protonation of the primary amines of the glucosamine residues as the endosome matures and becomes more acidic, which leads to a high charge density, membrane destabilization, and release of the particles. The charge density of chitosan is dependent on pH and the amount of deacetylation. In the present study, we chose a highly deacetylated chitosan complex with 86% of the monomers containing primary amines. Release of chitosan–SPION aggregates may also be

mediated by cationic mono- or di-saccharides that appear as chitosan is degraded by endosomal/lysosomal enzymes, such as lysozyme and N-acetyl-glucosamidase.^[15] However, as presented later, sustained cellular viability of these cells argues against lysosomal disruption, indicating that release of chitosan–SPIONs is either from non-lysosomal compartments or that membrane permeability is repaired following particle release.^[25]

When chitosan-coated SPIONs were incubated with macrophages in the absence of silicon particles (48 h), the majority of internalized SPIONs were located in electron dense clusters surrounded by membrane bilayers (Supporting Information, Figure 2). The contrast in localization of free, compared to LEV-delivered, chitosan-SPIONs indicates that the silicon particle may protect the surface coating of chitosan-SPIONs prior to cellular uptake, thus enhancing chitosan-mediated endosomal escape of SPIONs.

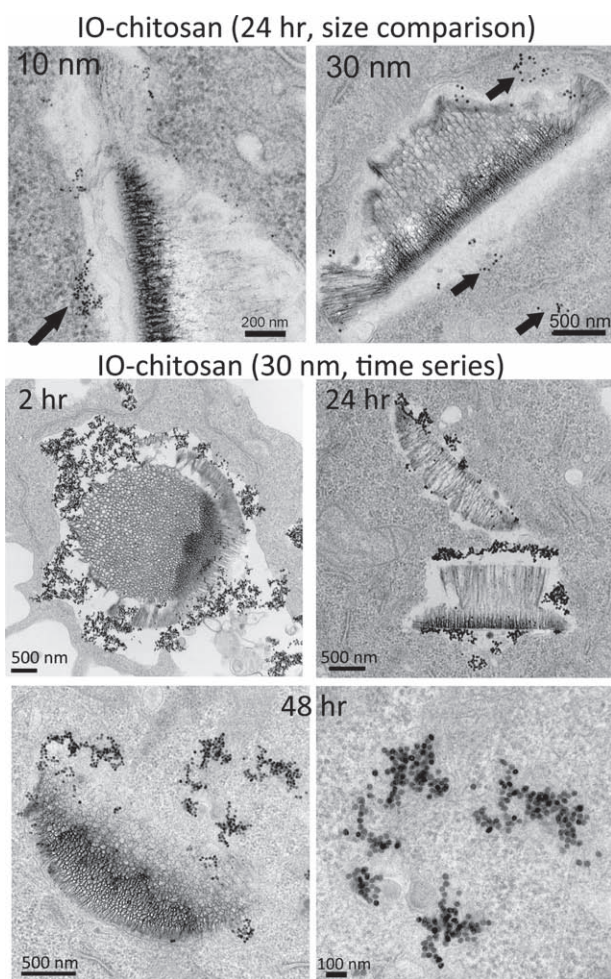


Figure 5. Intracellular trafficking of LEVs. Top row: TEM images of macrophage-internalized LEVs 24 h after particle introduction. LEVs were sparsely loaded with 10-nm (left, magnification 100 k) or 30-nm (right, 25 k) chitosan-coated nanoparticles (IO-chitosan). Bottom quadrant: time sequence of events for endosomal escape of 30-nm chitosan-SPIONs [magnification 25 k (top row), 50 k (bottom left), and 100 k (bottom right)].

2.5. Exocytosis of PEGylated Amine-SPIONs

We have previously demonstrated that LEVs composed of 10-nm amine-SPIONs and silicon particles are internalized by macrophages and endothelial cells into membrane-bound phagosomes/endosomes.^[23] Based on the presence of amine-SPION clusters in endosomal regions rich in MVBs 24 h after cellular uptake, we hypothesized that silicon carrier-released SPIONs were being actively sorted in the endosome. In **Figure 6a**, ultrathin sections of macrophages support active sorting of SPIONs into MVBs.

Ultrastructural examination of macrophages 6 days after LEV (silicon carriers and 15-nm amine-SPIONs) introduction (**Figure 6b**) revealed both intracellular and extracellular vesicles containing MVBs and SPIONs. The MVB and the exosome, approximately 1.5 μm in diameter, are further magnified in the images to the right of the cell. Within the endosome, SPIONs are visible in the region of the vesicle adjacent to the plasma membrane. A second exosome,

of similar size, is shown wrapped in the filopodia of a cell that was incubated with silicon particles loaded with 30-nm SPIONs (**Figure 6d**). The cellular morphology is consistent with healthy cells with no evidence of chromosome condensation or blebbing that would be expected with formation of cellular microparticles. The presence of membrane-bound compartments (MVBs) containing SPIONs near the plasma membrane (middle image in **Figure 6b**) suggests that fusion of MVBs with the plasma membrane may be the mechanism for cargo secretion, similar to that of exosomes.^[13] We recently reported endosomal sorting and exocytosis of amine-functionalized SPIONs by endothelial cells.^[26]

Based on the TEM images supporting secretion of novel membrane-bound compartments containing amine-SPIONs, and reports of eukaryotic cell-derived vectors containing SPIONs,^[27] as well as studies demonstrating exocytosis of nanoparticles in animal cells,^[28–30] we measured iron content in the supernatant of cells treated with LEVs containing either 15- or 30-nm SPIONs. Prussian blue quantitation of iron in the cell culture media was consistent with release of both 15- and 30-nm SPIONs from macrophages on all days tested (2–7 days; **Figure 6c**). Iron present in the media of untreated cells was subtracted from the values shown in the presented data. The amount of SPIONs released from cells treated with 15-nm particles was greater than that of cells treated with 30-nm particles ($p < 0.03$), thus indicating greater release of the smaller SPIONs. This is consistent with findings by Chithrani and Chan^[28] in which a linear relationship between exocytosis of gold nanoparticles and size was reported. The release of SPIONs from macrophages, as determined by Prussian blue analysis, was 0.6 μg (15 nm) and 0.4 μg (30 nm) iron per 2×10^5 original cells over 7 days, or a release of 9% (15 nm) and 6% (30 nm) of the nanoparticles introduced. **Figure 6e** illustrates dynamic communication between two macrophages, which emphasizes the potentially important role that cell-derived vectors may have in intercellular communication.

2.6. Cytotoxicity Testing

The release of exosomes and cellular microparticles/microvesicles from cells has been described as a mechanism for intercellular communication and a possible means for propagation of an immune response. This is supported by the existence of microvesicles containing interleukin-1 β (IL-1 β) following cellular stimulation, and the presence of MHC and endocytosed material in exosomes derived from antigen-presenting cells. We therefore examined the release of proinflammatory cytokines from macrophages treated with each particle formulation. Chou et al.^[31] and Kim et al.^[32] have reported that free chitosan attenuates the production of proinflammatory cytokines, including tumor necrosis factor α (TNF- α), IL-1 β , and IL-6. They also reported that 264.7 macrophages exhibit an increase in secretion of the anti-inflammatory cytokine IL-10. In our study, basal levels of interferon- γ (IFN- γ), IL-9, and IL-1 α were not affected

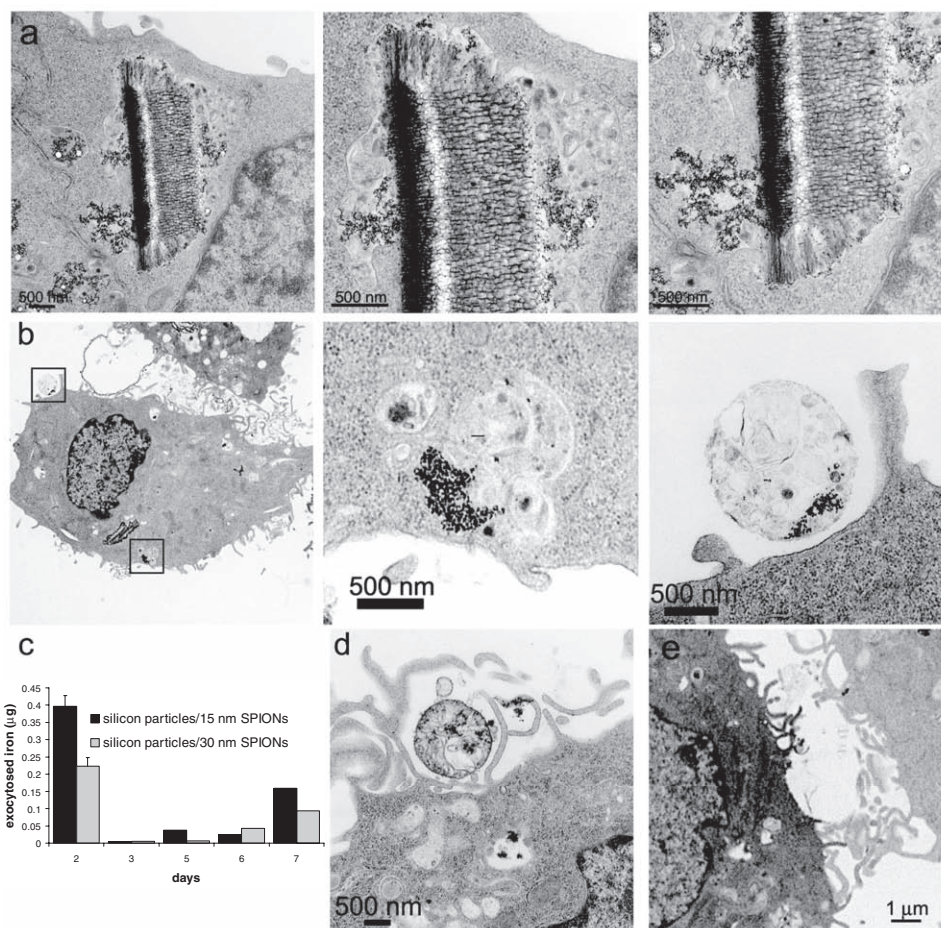


Figure 6. Exocytosis of MVBs carrying amine-SPIONs. a) TEM images of a macrophage-internalized LEV 24 h after introduction of LEVs to cells. Different regions of the LEV are shown to illustrate the formation of SPION-rich MVBs within the endosome (magnification: left, 25 k; middle, 50 k; and right, 50 k). b) TEM images of a macrophage 6 days after cellular uptake of silicon particles loaded with 15-nm amine-SPIONs (magnification: left, 6 k; middle, 25 k; and right, 50 k). c) Fe content in cell culture media 2–7 days following treatment with silicon particles loaded with either 15- or 30-nm amine-SPIONs. d) Macrophage treated with silicon particles carrying 30-nm amine-SPIONs, day 6 (25 k magnification). e) Intercellular communication between two macrophages.

by any of the particle formulations. However, at the 24 h time point, secretion of IL-6, TNF- α , and monocyte chemoattractant protein-1 (MCP-1) by macrophages was significantly reduced in cells incubated with chitosan-coated SPIONs and silicon particles loaded with either amine- or chitosan-coated SPIONs (Figure 7a). MCP-1 secretion was also reduced in cells incubated with unloaded silicon particles. Therefore it appears that the combination of SPIONs with either chitosan or silicon particles suppresses secretion of proinflammatory cytokines. These cytokines have been shown to have a prominent role in the progression of cancer and atherosclerosis, and a decrease in their production may have potential clinical implications.

A second test of cytotoxicity was performed by measuring cellular proliferation in the presence of each particle formulation. Macrophages were incubated for 24–96 h with either 10- or 30-nm free SPIONs ($1 \mu\text{g mL}^{-1}$), porous silicon microparticles ($2 \mu\text{g mL}^{-1}$), or LEVs (Figure 7b). None of the particle formulations had an impact on cellular proliferation. It has been reported that chitosan-coated SPIONs

impact proliferation only at concentrations greater than $200 \mu\text{g mL}^{-1}$ ^[33] and that Ferumoxtran-10 SPIONs are not toxic at 1 mg mL^{-1} and only mildly toxic at 10 mg mL^{-1} .^[34]

3. Discussion

Intracellular partitioning of particles in endosomes is summarized in the schematic shown in Figure 1. LEVs are internalized predominately as single units per phagosome, but occasionally as multiple units per phagosome. Endosomal sorting of particles is accompanied by the formation of MVBs. Membrane extension and formation of hourglass structures appear to be related to dissociation of SPION/MVB-rich regions of the phagosome, with formation of unique membrane-bound compartments that are candidates for exocytosis. Silicon microparticles display persistent perinuclear vesicular trafficking, while endosomal release of chitosan-coated SPIONs results in cytoplasmic localization of SPIONs. Delivery of chitosan-coated SPIONs within silicon

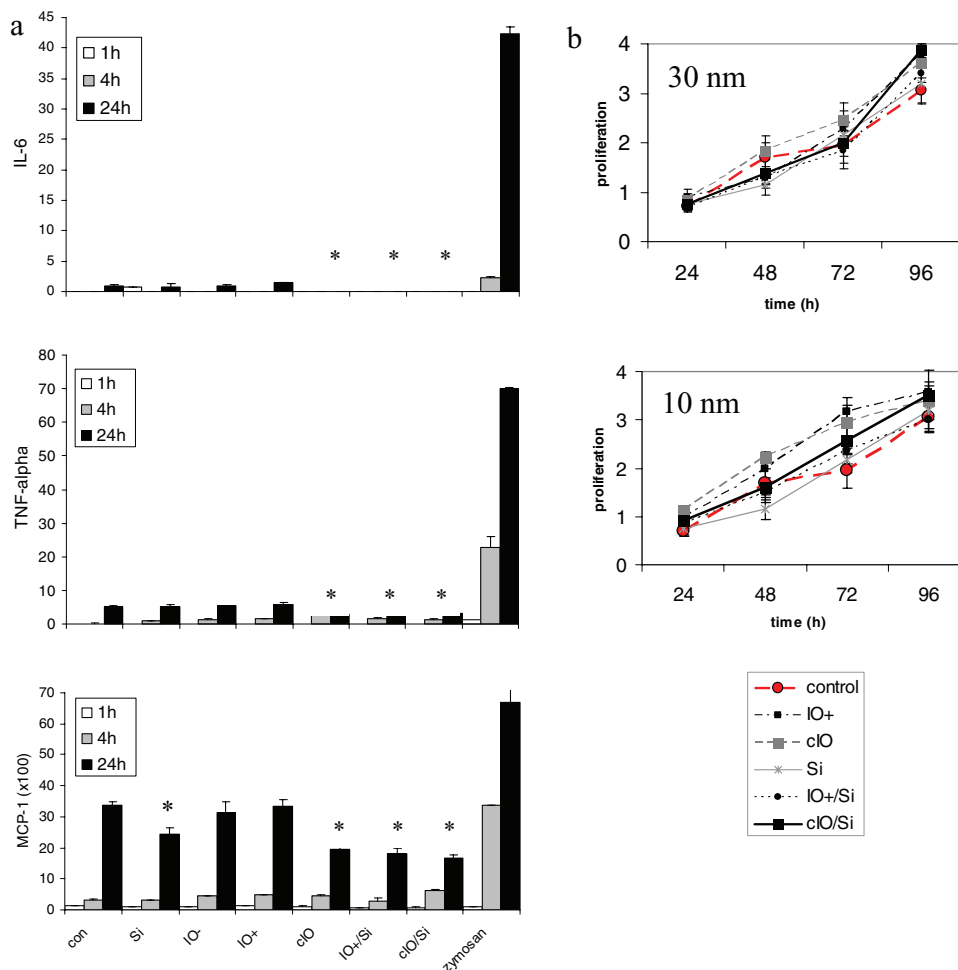


Figure 7. Cellular compatibility of LEVs. a) Secretion of cytokines by macrophages at 1, 4, and 24 h after introduction of particles. Secretion of IL-6, TNF- α , and MCP-1 by macrophages was significantly reduced in cells incubated with chitosan-coated SPIONs (cIO; $p < 0.03$, $p < 0.05$, and $p < 0.02$, respectively) and silicon particles loaded with amine (IO+/Si; $p < 0.04$, $p < 0.05$, and $p < 0.001$) and chitosan-coated (cIO/Si; $p < 0.006$, $p < 0.009$, and $p < 0.00006$) SPIONs. MCP-1 secretion was also reduced in cells incubated with unloaded silicon particles (Si; $p < 0.007$). b) MTT proliferation assays of macrophages incubated with each particle formulation across 4 days using two sizes of SPIONs (10 and 30 nm).

particles enhances endosomal escape compared to delivery of free chitosan-coated SPIONs, which supports a role for encapsulation in protecting nanoparticle surface coatings.

4. Conclusion

These results support the concept of LEVs, in which particle attributes are able to dictate unique intracellular and extracellular locations based on size and surface-tailored properties of the particles. Nested vectors thus create opportunities for coordinated and synergistic modulation of intracellular functions and a mechanism for cell–cell transport of therapeutics and imaging agents by means of cell-derived vectors.

5. Experimental Section

Silicon particle fabrication and surface modification: Porous silicon particles were fabricated in the Microelectronics Research Center at The University of Texas at Austin. Silicon particles, fea-

turing a mean diameter of $3.2 \pm 0.2 \mu\text{m}$ and an average pore size of 51.3 nm, were fabricated by protocols recently published by our laboratory.^[21,23] Briefly, heavily doped p++ type (100) silicon wafers with resistivity 0.005 $\Omega\text{-cm}$ (Silicon Quest, Inc., Santa Clara, CA) were used as the silicon source. A SiO_2 layer was thermally grown on the wafer, followed by a layer of silicon nitride (SiN) deposited by low-pressure chemical vapor deposition. Standard photolithography, a dry etch of SiN in CF_4 plasma, and a wet SiO_2 etch in 5% HF were used to transfer a pattern of 2- μm circle arrays on the silicon wafer. Silicon particles consisting of a low-porosity mechanical stabilization layer, large-pore device layer, and high-porosity release layer were then formed by a three-step electrochemical etch.^[21] The masking SiN and SiO_2 layers were removed in aqueous HF solution, and the silicon particles were released from the substrate by sonication in isopropanol (IPA).

Microparticles were treated with piranha solution (1 volume H_2O_2 and 2 volumes H_2SO_4) to chemically oxidize the surface. The suspension was heated to 110–120 $^\circ\text{C}$ for 2 h, centrifuged, and washed in deionized water repeatedly. For fluorescence microscopy experiments, 3-aminopropyltriethoxysilane (APTES; Sigma–Aldrich, St. Louis, MO)-modified particles were conjugated

to DyLight 594 (Pierce), an NHS ester-activated fluorescent dye, according to the manufacturer's protocol. APTES polymerization was performed using a 2% (v/v) APTES solution in 95% IPA and 5% water for 2 h at 35 °C with agitation at 1300 rpm.

Functionalization of SPIONs with chitosan: Chitosan (Protasan UP CL 113; 130 kDa, 86% deacetylated; Novamatrix, Norway) was dissolved at 30 mg mL⁻¹ in 50 mM borate buffer of pH 5.0. Chitosan was added to SPIONs (50 µg; Fe₃O₄, magnetite; 10, 15 or 30 nm; Ocean NanoTech, LLC, Springdale, AR), with vortexing, at equal volumes using 0.001–0.3% (w/v) chitosan and 0.1% (w/v) SPIONs for 1 h at room temperature. For cell assays, SPIONs were coated with a 0.03% (w/v) solution of chitosan at a 1:0.6 mass ratio of SPIONs to chitosan. Unbound chitosan was removed with either a MACS magnetic purification column (Miltenyi Biotec, Germany) using 500–2000 mL borate buffer for washing and 200 µL for removal of bound particles, or by magnetic collection using a SuperMag Multi-tube Separator (Ocean Nanotech) and two 500 µL washes.

Quantitation of chitosan coating: The number of chitosan molecules per SPION after purification was determined using a colorimetric assay adapted from Muzzarelli.^[35] Briefly, SPIONs were coated with different concentrations of chitosan (0–3 mg mL⁻¹) using the protocol described above. After filtering, aliquots (20 µL, 5 µg) of coated SPIONs were raised to 150 µL using a glycine–HCl buffer (80 mM glycine, 80 mM NaCl, and 20 mM HCl; Sigma–Aldrich). Samples were diluted 1:1 using freshly prepared 0.3% (w/v) Congo Red dye (Sigma–Aldrich) in water. Absorbance values were immediately measured at 520 nm using a BioTek Synergy 4 Hybrid plate reader (Winooski, VT). Standard curves were generated using free chitosan and unfiltered cIO coated with known concentrations of chitosan, both treated with dye, and uncoated IO diluted to 300 µL using glycine–HCl. The mean number of chitosan molecules was determined from a fit to the standard curves, averaged across three independent experiments.

DLS and zeta potential analysis: A ZetaPALS zeta potential analyzer equipped with a 90Plus/BI-MAS multiangle particle sizing option (Brookhaven Instruments Corp., Holtsville, NY) was used to measure the mean particle diameter and zeta potentials using borate buffer of pH 5.0 as the solvent. Conditions for DLS sample measurements were 25 °C at a 90° angle for 2 min per measurement with water as the solvent used for calculation. The refractive index of the particles was set to 1.4 and the dust cutoff filter was set to 50. Each final measurement is four 2 - min measurements averaged together.

FTIR spectroscopy: Samples were prepared for FTIR spectroscopy by magnetic purification and washing with 0.1% acetic acid. Wash samples were resuspended in 0.1% acetic acid (1 mL) and a portion (1 µL) was applied to the diamond surface of a SMART attenuated total reflection (ATR) attachment on a Nicolet 6600 FTIR spectrometer. The applied sample was then dried with dry nitrogen and the FTIR spectra were read. A room-temperature detector was used to collect all data, and all readings were made using a resolution of 4 and by averaging 16 readings in absorbance mode to form an absorbance curve. Analysis of the peaks was performed using Omnic peak identification software and with Microsoft Excel.

Loading silicon particles: Assembly of the LEV was previously published by our group.^[23] Briefly, oxidized silicon particles (5 × 10⁶) were dried overnight at room temperature in a vacuum desiccator. Fe₃O₄ nanoparticles (40 µg) (carboxylated and amine-functionalized nanoparticles were purchased from Ocean NanoTech,

LLC, Springdale, AR) were added to the dry silicon particles in borate buffer at 0.5–1.0 mg mL⁻¹. The particle suspension was briefly sonicated and incubated for 30 min with intermittent mixing (1300 rpm). Samples were then centrifuged at 4200 rpm (Beckman Coulter Allegra X-22 centrifuge equipped with a 296/06 rotor) to remove free iron oxide nanoparticles, followed by washing twice with borate buffer. Loaded silicon particles were suspended in cell culture media and incubated with J774 cells for the indicated amount of time.

Live confocal microscopy: J77A cells were cultured in glass-bottomed 24-well plates purchased from MatTek Corporation (Ashland, MA). CellTracker Green CMFDA (Molecular Probes, Eugene, OR) was introduced to the cells at a concentration of 0.5 µM in serum-free medium for 30 min at 37 °C, followed by another 30 min in fresh medium at 37 °C. DyLight 594-modified microparticles (1:10 cell:microparticle) were added to the culture, and images were acquired in four z-planes with a step size of 1.5 µm every 3 min using a 1 × 81 Olympus microscope equipped with a DSU confocal attachment and a 40× water-immersion objective. Still shots represent the best focal plane while the movie is comprised of projection images using in-focus light from all planes.

MTT cell proliferation assay: J774 cells, purchased from American Type Culture Collection (Manassas, VA), were cultured in Dulbecco's modified Eagle's medium containing 10% fetal bovine serum (FBS), 100 µg mL⁻¹ streptomycin, and 100 U mL⁻¹ penicillin (Invitrogen, Carlsbad, CA). J774 cells were seeded into 96-well plates at 5000 cells well⁻¹ in a final volume of 200 µL well⁻¹. Twenty-four hours later, media containing silicon particles (either unloaded or loaded with SPIONs, with and without chitosan coating) were added at a ratio of 1:10 cells to microparticles. Free SPIONs were incubated with cells at a concentration of 1 µg mL⁻¹. At 24, 48, 72, and 96 h, the medium was removed and medium containing 3-(4,5-dimethylthiazol-2-yl)-2,5-diphenyltetrazolium bromide (0.5 mg mL⁻¹; MTT; Sigma–Aldrich) was added at 200 µL well⁻¹ for 4 h at 37 °C to the appropriate plates. Medium was then removed and dimethyl sulfoxide (180 µL well⁻¹) was added to each well. After 30 min at room temperature, the absorbance was read at 570 nm using a SPECTRA max M2 plate reader (Molecular Devices).

Cytokine analysis: J774 macrophages were cultured overnight in 24-well plates (1 × 10⁵ cells well⁻¹) containing 1 mL medium. After 24 h, the cells were incubated with fresh medium containing unloaded silicon particles or silicon particles loaded with SPION variants (10 particles cell⁻¹). Zymosan (20 µg mL⁻¹; Sigma, USA) were used as a positive control for cytokines production and untreated cells were used as a measure of basal levels of cytokine release. The cell culture supernatant (300 µL) was collected at 1, 4, and 24 h and stored at –80 °C. Samples were analyzed according to the manufacturer's instructions using a Milliplex mouse 10-cytokine assay panel. The following cytokines were assessed: IFN-γ, IL-1β, IL-2, IL-6, IL-9, KC, MCP-1, RANTES, and TNF-α. Cytokine levels were read on the Luminex 200 System, Multiplex Bioassay Analyzer. The quantification was carried out based on standard curves for each cytokine in the concentration range of 1–32 000 pg mL⁻¹.

SEM: J774 cells were plated in 24-well plates containing 5 mm × 7 mm silicon chip specimen supports (Ted Pella, Inc., Redding, CA) at 5 × 10⁴ cells per well. When cells were confluent, serum-free media containing oxidized silicon particles (1:10, cell:microparticles, 0.5 mL well⁻¹) were introduced and the cells were incubated at 37 °C for 15 min. Samples were washed with phosphate-buffered saline (PBS) and fixed in 2.5% glutaraldehyde

for 30 min (Sigma–Aldrich, St. Louis, MO). Samples were processed and imaged as described previously.^[23] Micrographs were acquired under high vacuum at 20–30 kV, spot size 3.0–5.0, using either an FEI Quanta 400 FEG ESEM instrument equipped with an ETD (SE) detector or a Hitachi S-5500 SEM apparatus.

TEM: J774 cells were grown to 80% confluency in a six-well plate. Using 1–2 mL of medium per well, particles were introduced as described previously (e.g., silicon particles 10:1) at 37 °C for either 15 min, or 2, 24, 48, or 144 h. The cells were then washed and fixed in a solution of 2% paraformaldehyde (Electron Microscopy Sciences, Hatfield, PA) and 3% glutaraldehyde (Sigma–Aldrich) in PBS of pH 7.4 for 1 h at room temperature. Samples were processed and imaged as described previously.^[23]

Quantitation of nanoparticle exocytosis: J774 cells were incubated with particles as described in the preceding paragraph. At 48, 96, 120, and 144 h the medium was removed and centrifuged at 14 000 rpm for 20 min. The pellets were washed in PBS and resuspended in 6N HCl (50 µL) followed by incubation at 60 °C for 2 h. Iron was then oxidized using ammonium persulfate (0.1 mg mL⁻¹; BioRad, Richmond, CA) and the color reaction was initiated by adding 5% K₄[Fe(CN)₆]·3H₂O (50 µL; Sigma–Aldrich) for 10 min. A standard curve was generated using iron(III) hexahydrate (Sigma–Aldrich), and the absorbance was read at 690 nm using a SPECTRA max M2 plate reader (Molecular Devices).

Supporting Information

Supporting Information is available from the Wiley Online Library or from the author. Supporting Video: DyLight 594-modified silicon particles were introduced to CellTracker Green CMFDA-stained macrophages and images were acquired every 3 min using a 1 × 81 Olympus microscope equipped with a DSU confocal attachment and a 40× water-immersion objective at 37 °C.

Acknowledgements

A.M. and A.L.vdV. contributed equally to this work. We thank Hitachi for training and use of the S-5500 high-resolution scanning electron microscope. Live cell imaging was performed at the UT-MDACC shared microscopy facility with the much appreciated assistance of Jared K. Burks. This research was supported by the Department of Defense grants DODW81XWH-07-1-0596 and DODW81XWH-09-1-0212; NASA NNJ06HE06A; NIH RO1CA128797, U54CA143837, MH58920, and RC2GM092599; MDACC Institutional Core Grant #CA-016672; and The State of Texas, Emerging Technology Fund.

- [1] B. R. Selvi, D. Jagadeesan, B. S. Suma, G. Nagashankar, M. Arif, K. Balasubramanyam, M. Eswaramoorthy, T. K. Kundu, *Nano Lett.* **2008**, *8*, 3182–3188.
- [2] A. Hoshino, K. Fujioka, T. Oku, S. Nakamura, M. Suga, Y. Yamaguchi, K. Suzuki, M. Yasuhara, K. Yamamoto, *Microbiol. Immunol.* **2004**, *48*, 985–994.
- [3] P. Nativo, I. A. Prior, M. Brust, *ACS Nano* **2008**, *2*, 1639–1644.
- [4] T. Xia, M. Kovochich, M. Liong, J. I. Zink, A. E. Nel, *ACS Nano* **2008**, *2*, 85–96.

- [5] M. Jovic, M. Sharma, J. Rahajeng, S. Caplan, *Histol. Histopathol.* **2010**, *25*, 99–112.
- [6] C. C. Scott, R. J. Botelho, S. Grinstein, *J. Membr. Biol.* **2003**, *193*, 137–152.
- [7] T. J. Greenwalt, *Transfusion* **2006**, *46*, 143–152.
- [8] A. M. Kaufmann, J. P. Krise, *J. Biol. Chem.* **2008**, *283*, 24584–24593.
- [9] K. Denzer, M. J. Kleijmeer, H. F. Heijnen, W. Stoorvogel, H. J. Geuze, *J. Cell Sci.* **2000**, *113* (Pt. 19)3365–3374.
- [10] W. Kolowos, U. S. Gaipal, A. Sheriff, R. E. Voll, P. Heyder, P. Kern, J. R. Kalden, M. Herrmann, *Scand. J. Immunol.* **2005**, *61*, 226–233.
- [11] V. Combes, A. C. Simon, G. E. Grau, D. Arnoux, L. Camoin, F. Sabatier, M. Mutin, M. Sanmarco, J. Sampol, F. Dignat-George, *J. Clin. Invest.* **1999**, *104*, 93–102.
- [12] P. Siljander, R. W. Farndale, M. A. Feijge, P. Comfurios, S. Kos, E. M. Bevers, J. W. Heemskerker, *Arterioscler. Thromb. Vasc. Biol.* **2001**, *21*, 618–627.
- [13] J. Wolfers, A. Lozier, G. Raposo, A. Regnault, C. Thery, C. Masurier, C. Flament, S. Pouzieux, F. Faure, T. Tursz, E. Angevin, S. Amigorena, L. Zitvogel, *Nat. Med.* **2001**, *7*, 297–303.
- [14] B. Fevrier, D. Vilette, H. Laude, G. Raposo, *Traffic* **2005**, *6*, 10–17.
- [15] M. Koping-Hoggard, I. Tubulekas, H. Guan, K. Edwards, M. Nilsson, K. M. Varum, P. Artursson, *Gene Ther.* **2001**, *8*, 1108–1121.
- [16] A. J. Ditto, P. N. Shah, L. R. Gump, Y. H. Yun, *Mol. Pharm.* **2009**, *6*, 986–995.
- [17] B. Albarran, R. To, P. S. Stayton, *Protein Eng. Des. Sel.* **2005**, *18*, 147–152.
- [18] C. A. Lackey, O. W. Press, A. S. Hoffman, P. S. Stayton, *Bioconjugate Chem.* **2002**, *13*, 996–1001.
- [19] X. Yin, A. S. Hoffman, P. S. Stayton, *Biomacromolecules* **2006**, *7*, 1381–1385.
- [20] N. Sarkar, J. Banerjee, A. J. Hanson, A. I. Elegbede, T. Rosendahl, A. B. Krueger, A. L. Banerjee, S. Tobwala, R. Wang, X. Lu, S. Mallik, D. K. Srivastava, *Bioconjugate Chem.* **2008**, *19*, 57–64.
- [21] C. Chiappini, E. Tasciotti, J. R. Fakhoury, D. Fine, L. Pullan, Y. C. Wang, L. Fu, X. Liu, M. Ferrari, *ChemPhysChem* **2010**, *11*, 1029–1035.
- [22] R. E. Serda, J. Gu, J. K. Burks, K. Ferrari, C. Ferrari, M. Ferrari, *Cytometry A* **2009**, *75*, 752–760.
- [23] R. E. Serda, A. Mack, M. Pulikkathara, A. M. Zaske, C. Chiappini, J. R. Fakhoury, D. Webb, B. Godin, J. L. Conyers, X. W. Liu, J. A. Bankson, M. Ferrari, *Small* **2010**, *6*, 1329–1340.
- [24] J. S. Park, T. H. Han, K. Y. Lee, S. S. Han, J. J. Hwang, D. H. Moon, S. Y. Kim, Y. W. Cho, *J. Controlled Release* **2006**, *115*, 37–45.
- [25] B. Ghosn, A. L. van de Ven, J. Tam, A. Gillenwater, K. V. Sokolov, R. Richards-Kortum, K. Roy, *J. Biomed. Opt.* **2010**, *15*, 015003.
- [26] S. Ferrati, A. Mack, C. Chiappini, X. Liu, A. J. Bean, M. Ferrari, R. E. Serda, *Nanoscale* **2010**, *2*, 1512–1520.
- [27] C. Wilhelm, F. Lavielle, C. Pechoux, I. Tatischeff, F. Gazeau, *Small* **2008**, *4*, 577–582.
- [28] B. D. Chitrani, W. C. Chan, *Nano Lett.* **2007**, *7*, 1542–1550.
- [29] P. Walczak, D. A. Kedziorek, A. A. Gilad, B. P. Barnett, J. W. Bulte, *Magn. Reson. Med.* **2007**, *58*, 261–269.
- [30] J. Panyam, V. Labhasetwar, *Pharm. Res.* **2003**, *20*, 212–220.
- [31] T. C. Chou, E. Fu, E. C. Shen, *Biochem. Biophys. Res. Commun.* **2003**, *308*, 403–407.
- [32] M. S. Kim, M. J. Sung, S. B. Seo, S. J. Yoo, W. K. Lim, H. M. Kim, *Neurosci. Lett.* **2002**, *321*, 105–109.
- [33] A. M. Reddy, B. K. Kwak, H. J. Shim, C. Ahn, H. S. Lee, Y. J. Suh, E. S. Park, *J. Korean Med. Sci.* **2010**, *25*, 211–219.
- [34] K. Muller, J. N. Skepper, M. Posfai, R. Trivedi, S. Howarth, C. Corot, E. Lancelot, P. W. Thompson, A. P. Brown, J. H. Gillard, *Biomaterials* **2007**, *28*, 1629–1642.
- [35] R. A. Muzzarelli, *Anal. Biochem.* **1998**, *260*, 255–257.

Received: April 29, 2010

Revised: July 22, 2010

Published online: October 18, 2010